Research Article | Vol. 26, No. 3 | 5 Feb 2018 | OPTICS EXPRESS 3221

Optics EXPRESS

Carbon chloride-core fibers for soliton mediated supercontinuum generation

MARIO CHEMNITZ,[1,*] CHRISTIAN GAIDA,[2] MARTIN GEBHARDT,[2,3] FABIAN STUTZKI,[2,4] JENS KOBELKE,[1] ANDREAS TÜNNERMANN,[2,3,4] JENS LIMPERT,[2,3,4] AND MARKUS A. SCHMIDT[1,5]

[1]*Leibniz Institute of Photonic Technology, Abbe Center of Photonics, Albert-Einstein-Str. 9, 07745 Jena, Germany*
[2]*Institute of Applied Physics, Abbe Center of Photonics, Friedrich-Schiller-University Jena, Albert-Einstein-Str. 15, 07745 Jena, Germany*
[3]*Helmholtz-Institute Jena, Froebelstieg 3, 07743 Jena, Germany*
[4]*Fraunhofer Institute for Applied Optics and Precision Engineering, Albert-Einstein-Str. 7, 07745 Jena, Germany*
[5]*Otto Schott Institute of Material Research, Abbe Center of Photonics, Friedrich Schiller University of Jena, Fraunhoferstrasse 6, 07743 Jena, Germany*
[*]*mario.chemnitz@leibniz-ipht.de*

Abstract: We report on soliton-fission mediated infrared supercontinuum generation in liquid-core step-index fibers using highly transparent carbon chlorides (CCl_4, C_2Cl_4). By developing models for the refractive index dispersions and nonlinear response functions, dispersion engineering and pumping with an ultrafast thulium fiber laser (300 fs) at 1.92 µm, distinct soliton fission and dispersive wave generation was observed, particularly in the case of tetrachloroethylene (C_2Cl_4). The measured results match simulations of both the generalized and a hybrid nonlinear Schrödinger equation, with the latter resembling the characteristics of a non-instantaneous medium via a static potential term and representing a simulation tool with substantially reduced complexity. We show that C_2Cl_4 has the potential for observing non-instantaneous soliton dynamics along meters of liquid-core fiber opening a feasible route for directly observing hybrid soliton dynamics.

OCIS codes: (060.4370) Nonlinear optics, fibers; (060.2390) Fiber optics, infrared; (190.4400) Nonlinear optics, materials; (190.5530) Pulse propagation and temporal solitons; (320.6629) Supercontinuum generation.

References and links

1. U. Willer, M. Saraji, A. Khorsandi, P. Geiser, and W. Schade, "Near- and mid-infrared laser monitoring of industrial processes, environment and security applications," Opt. Laser Eng. **44**, 699–710 (2006).
2. A. Schliesser, N. Picqué, and T. W. Hänsch, "Mid-infrared frequency combs," Nat. Photonics **6**, 440–449 (2012).
3. M. A. Schmidt, A. Argyros, and F. Sorin, "Hybrid Optical Fibers - An Innovative Platform for In-Fiber Photonic Devices," Adv. Opt. Mater. **4**, 13–36 (2016).
4. C. R. Petersen, U. Møller, I. Kubat, B. Zhou, S. Dupont, J. Ramsay, T. Benson, S. Sujecki, N. Abdel-Moneim, Z. Tang, D. Furniss, A. Seddon, and O. Bang, "Mid-infrared supercontinuum covering the 1.4–13.3 μm molecular fingerprint region using ultra-high NA chalcogenide step-index fibre," Nat. Photonics **8**, 830–834 (2014).
5. S. Xie, F. Tani, J. C. Travers, P. Uebel, C. Caillaud, J. Troles, M. A. Schmidt, and P. S. Russell, "As_2S_3-silica double-nanospike waveguide for mid-infrared supercontinuum generation," Opt. Lett. **39**, 5216–5219 (2014).
6. K. F. Mak, J. C. Travers, P. Holzer, N. Y. Joly, and P. S. Russell, "Tunable vacuum-UV to visible ultrafast pulse source based on gas-filled Kagome-PCF," Opt. Express **21**, 10942–10953 (2013).
7. M. Gebhardt, C. Gaida, F. Stutzki, S. Hädrich, C. Jauregui, J. Limpert, and A. Tünnermann, "High average power nonlinear compression to 4GW, sub-50fs pulses at 2μm wavelength," Opt. Lett. **42**, 747–750 (2017).
8. R. Sollapur, D. Kartashov, M. Zürch, A. Hoffmann, T. Grigorova, G. Sauer, A. Hartung, A. Schwuchow, J. Bierlich, J. Kobelke, M. Chemnitz, M. A. Schmidt, and C. Spielmann, "Resonance-enhanced multi-octave supercontinuum generation in antiresonant hollow-core fibers," Light: Sci. Appl. **6**, e17124 (2017).
9. F. Tani, J. C. Travers, and P. S. J. Russell, "PHz-wide Supercontinua of Nondispersing Subcycle Pulses Generated by Extreme Modulational Instability," Phys. Rev. Lett. **111**, 033902 (2013).

#309416 https://doi.org/10.1364/OE.26.003221
Journal © 2018 Received 18 Oct 2017; revised 8 Dec 2017; accepted 9 Dec 2017; published 30 Jan 2018
Corrected: 19 March 2018

Optics EXPRESS

10. F. Belli, A. Abdolvand, W. Chang, J. C. Travers, and P. S. J. Russell, "Vacuum-ultraviolet to infrared supercontinuum in hydrogen-filled photonic crystal fiber," Optica **2**, 292–300 (2015).
11. M. I. Hasan, N. Akhmediev, and W. Chang, "Mid-infrared supercontinuum generation in supercritical xenon-filled hollow-core negative curvature fibers," Opt. Lett. **41**, 5122–5125 (2016).
12. S. Kedenburg, M. Vieweg, T. Gissibl, and H. Giessen, "Linear refractive index and absorption measurements of nonlinear optical liquids in the visible and near-infrared spectral region," Opt. Mat. Express **2**, 1588–1611 (2012).
13. M. Plidschun, M. Chemnitz, and M. A. Schmidt, "Low-loss deuterated organic solvents for visible and near-infrared photonics," Opt. Mat. Express **7**, 1122–1130 (2017).
14. P. P. Ho, R. R. Alfano, "Optical Kerr effect in liquids," Phys. Rev. A **20**, 2170–2187 (1979).
15. F. I. Mopsik, "Dielectric Properties of Slightly Polar Organic Liquids as a Function of Pressure, Volume, and Temperature," J. Chem. Phys. **50**, 2559–2569 (1969).
16. L. Velázquez-Ibarra, A. Díez, E. Silvestre, and M. V. Andrés, "Wideband tuning of four-wave mixing in solid-core liquid-filled photonic crystal fibers," Opt. Lett. **41**, 2600–2603 (2016).
17. S. Pumpe, M. Chemnitz, J. Kobelke, and M. A. Schmidt, "Monolithic optofluidic mode coupler for broadband thermo- and piezo-optical characterization of liquids," Opt. Express **25**, 22932–22946 (2017).
18. G. S. He, M. Casstevens, R. Burzynski, and X. Li, "Broadband, multiwavelength stimulated-emission source based on stimulated Kerr and Raman scattering in a liquid-core fiber system," Appl. Optics **34**, 444–454 (1995).
19. S. Yiou, P. Delaye, A. Rouvie, J. Chinaud, R. Frey, G. Roosen, P. Viale, S. Février, P. Roy, J.-L. Auguste, and J.-M. Blondy, "Stimulated Raman scattering in an ethanol core microstructured optical fiber," Opt. Express **13**, 4786–4791 (2005).
20. F. Dai, Y. Xu, and X. Chen, "Enhanced and broadened SRS spectra of toluene mixed with chloroform in liquid-core fiber," Opt. Express **17**, 19882–19886 (2009).
21. G. Fanjoux, A. Sudirman, J.-C. Beugnot, L. Furfaro, W. Margulis, and T. Sylvestre, "Stimulated Raman-Kerr scattering in an integrated nonlinear optofluidic fiber arrangement," Opt. Lett. **39**, 5407–5410 (2014).
22. D. Churin, T. Nguyen, K. Kieu, R. A. Norwood, and N. Peyghambarian, "Mid-IR supercontinuum generation in an integrated liquid-core optical fiber filled with CS_2," Opt. Mat. Express **3**, 1358–1364 (2013).
23. S. Kedenburg, T. Gissibl, T. Steinle, A. Steinmann, and H. Giessen, "Towards integration of a liquid-filled fiber capillary for supercontinuum generation in the 1.2-2.4μm range," Opt. Express **23**, 8281–8289 (2015).
24. A. Bozolan, C. J. de Matos, C. M. Cordeiro, E. M. Dos Santos, and J. Travers, "Supercontinuum generation in a water-core photonic crystal fiber," Opt. Express **16**, 9671–9676 (2008).
25. J. Bethge, A. Husakou, F. Mitschke, F. Noack, U. Griebner, G. Steinmeyer, and J. Herrmann, "Two-octave supercontinuum generation in a water-filled photonic crystal fiber," Opt. Express **18**, 6230–6240 (2010).
26. M. Chemnitz, M. Gebhardt, C. Gaida, F. Stutzki, J. Kobelke, J. Limpert, A. Tünnermann, and M. A. Schmidt, "Hybrid soliton dynamics in liquid-core fibres," Nat. Commun. **8**, 42 (2017).
27. D. McMorrow, W. Lotshaw, and G. Kenney-Wallace, "Femtosecond optical Kerr studies on the origin of the nonlinear responses in simple liquids," IEEE J. Quantum Elect. **24**, 443–454 (1988).
28. M. Reichert, H. Hu, M. R. Ferdinandus, M. Seidel, P. Zhao, T. R. Ensley, D. Peceli, J. M. Reed, D. A. Fishman, S. Webster, D. J. Hagan, and E. W. Van Stryland, "Temporal, spectral, and polarization dependence of the nonlinear optical response of carbon disulfide," Optica **1**, 436–445 (2014).
29. C. Conti, M. A. Schmidt, P. S. J. Russell, and F. Biancalana, "Highly Noninstantaneous Solitons in Liquid-Core Photonic Crystal Fibers," Phys. Rev. Lett. **105**, 263902 (2010).
30. M. C. Braidotti, A. Mecozzi, and C. Conti, "Squeezing in a nonlocal photon fluid," Phys. Rev. A **96**, 043823 (2017).
31. M. Vieweg, T. Gissibl, S. Pricking, B. T. Kuhlmey, D. C. Wu, B. J. Eggleton, and H. Giessen, "Ultrafast nonlinear optofluidics in selectively liquid-filled photonic crystal fibers," Opt. Express **18**, 25232–25240 (2010).
32. M. Vieweg, T. Gissibl, Y. V. Kartashov, L. Torner, and H. Giessen, "Spatial solitons in optofluidic waveguide arrays with focusing ultrafast Kerr nonlinearity," Opt. Lett. **37**, 2454–2456 (2012).
33. M. Vieweg, S. Pricking, T. Gissibl, Y. Kartashov, L. Torner, and H. Giessen, "Tunable ultrafast nonlinear optofluidic coupler," Opt. Lett. **37**, 1058–1060 (2012).
34. A. Majumdar, D. Hinkley, and R. Menzies, "Infrared transmission at the 3.39 μm helium-neon laser wavelength in liquid-core quartz fibers," IEEE J. Quantum Elect. **15**, 408–410 (1979).
35. S. Diemer, J. Meister, R. Jung, S. Klein, M. Haisch, W. Fuss, and P. Hering, "Liquid-core light guides for near-infrared applications," Appl. Optics **36**, 9075–9082 (1997).
36. J. Meister, R. Franzen, G. Eyrich, J. Bongartz, N. Gutknecht, and P. Hering, "First clinical application of a liquid-core light guide connected to an Er:YAG laser for oral treatment of leukoplakia," Laser Med. Sci. **25**, 669–673 (2010).
37. D. Mann, N. Acquista, and E. Plyler, "Vibrational spectra of tetrafluoroethylene and tetrachloroethylene," J. Res. Nat. Bur. Stand. **52**, 67–72 (1954).
38. N. Thantu and R. S. Schley, "Ultrafast third-order nonlinear optical spectroscopy of chlorinated hydrocarbons," Vib. Spectroscopy **32**, 215–223 (2003).
39. D. Lopez-Cortes, O. Tarasenko, and W. Margulis, "All-fiber Kerr cell," Opt. Lett. **37**, 3288–3290 (2012).
40. A. H. Pfund, "The Dispersion of CS_2 and CCl_4 in the Infrared," J. Opt. Soc. Am. **25**, 351 – 354 (1935).
41. S. Ghosal, J. L. Ebert, and S. A. Self, "The infrared refractive indices of $CHBr_3$, CCl_4 and CS_2," Infrared Phys. **34**, 621–628 (1993).
42. R. E. Kagarise, "Infrared Dispersion of Some Organic Liquids," J. Opt. Soc. Am. **50**, 36–39 (1960).

Optics EXPRESS

43. J. Vincent-Geisse, "Dispersion de quelques liquides organiques dans l'infrarouge. détermination des intensités de bandes et des polarisations," J. Phys. France **26**, 289–296 (1965).
44. J. Yarwood and W. J. Orville-Thomas, "Infra-red dispersion studies. Part 7 Band intensities and atomic polarizations of $CX_2 = CCl_2$(X = H, F, Cl) molecules," T. Faraday Soc. **62**, 3294–3309 (1966).
45. K. Spaeth, G. Kraus, and G. Gauglitz, "In-situ characterization of thin polymer films for applications in chemical sensing of volatile organic compounds by spectroscopic ellipsometry," Fresen. J. Anal. Chem. **357**, 292–296 (1997).
46. B. Wilhelmi, "Über die Anwendung von Dispersionsrelationen zur Bestimmung optischer Konstanten," Ann. Phys. **474**, 244–252 (1967).
47. A. Samoc, "Dispersion of refractive properties of solvents: Chloroform, toluene, benzene, and carbon disulfide in ultraviolet, visible, and near-infrared," J. Appl. Phys. **94**, 6167–6174 (2003).
48. R. H. Stolen, "Raman gain in glass optical waveguides," Appl. Phys. Lett. **22**, 276–278 (1973).
49. D. Hollenbeck and C. Cantrell, "Multiple-vibrational-mode model for fiber-optic Raman gain spectrum and response function," J. Opt. Soc. Am. B **19**, 2886–2892 (2002).
50. M. J. Weber, *Handbook of Optical Materials* (CRC, 2003).
51. P. Zhao, M. Reichert, T. R. Ensley, W. M. Shensky, A. G. Mott, D. J. Hagan, and E. W. Van Stryland, "Nonlinear refraction dynamics of solvents and gases," Proc. SPIE 9731 "Nonlinear Frequency Generation and Conversion: Materials, Devices, and Applications XV," 97310F (2016).
52. G. Agrawal, *Nonlinear Fiber Optics,* 5th ed. (Academic, 2013).
53. M. Chemnitz and M. A. Schmidt, "Single mode criterion - a benchmark figure to optimize the performance of nonlinear fibers," Opt. Express **24**, 16191–16205 (2016).
54. N. An, B. Zhuang, M. Li, Y. Lu, and Z.-G. Wang, "Combined Theoretical and Experimental Study of Refractive Indices of Water-Acetonitrile-Salt Systems," J. Phys. Chem. B **119**, 10701–10709 (2015).
55. J. Laegsgaard, "Mode profile dispersion in the generalized nonlinear Schrödinger equation," Opt. Express **15**, 16110–16123 (2007).
56. J. M. Dudley, G. Genty, and S. Coen, "Supercontinuum generation in photonic crystal fiber," Rev. Mod. Phys. **78**, 1135–1184 (2006).

1. Introduction

Near- to mid-infrared (N/MIR) photonics represents one of the driving sources for the upcoming innovations in fields such as environmental monitoring, health care, or industrial quality control [1]. Compact, tunable, and broadband nonlinear light sources, in particular those relying on supercontinuum generation, integrated in efficient waveguides play a key role in this development [2]. Hybrid-material optical fibers offer the potential to overcome the limitations of silica fibers in terms of transmission and optical nonlinearity by selectively combining favourable materials within one single fiber structure [3]. Examples of nonlinear light generation in fibers include soft-glass fibers for supercontinuum generation in the NIR to MIR at pico- to sub-microjoule pulse energies [4, 5], and gas-filled hollow-core fibers for ultrashort pulse generation in the ultraviolet (UV) or NIR wavelength region at pulse energies of microjoules and above [6, 7]. In addition to applications in the UV, the latter type of fiber also hosts many unexplored physical effects such as resonance-enhanced multiple phase-matching events [8], extreme instability events due to ionization effects [9], Raman-enhanced supercontinuum cascades [10], or enhanced nonlinearities at the supercritical limit [11].

Less known is the innovative potential of liquid-core fibers (LCF), which combines good transmission from visible to NIR wavelengths [12, 13] with nonlinearities as high as those of soft-glasses [14], and tuning capabilities comparable to those of gases [15–17]. The potential of LCFs for broadband light generation in the visible to the NIR has been demonstrated multiple times by harvesting either the strong Raman activity [18–21], or the strong nonlinearity in the normal [22, 23] or the anomalous dispersion regime [24–26]. Moreover liquids feature highly noninstantaneous nonlinearities [27, 28] being unique for liquids and promising the observation of novel states of light [26, 29, 30].

However, most of the organic solvents used in those experiments (i.e., water, ethanol, toluene) possess large losses towards the NIR [12, 13] limiting applications within N/MIR photonics. Analogous to specialized MIR glasses such as fluoride glasses, halogen-based liquids have significantly lower IR absorption. Due to the low refractive indices of flouride-based liquids and the high toxicity of bromides, the most commonly used halogenides for nonlinear photonics

Optics EXPRESS

for NIR applications are carbon chlorides. In particular, carbon tetrachloride (CCl_4, or CTC) was extensively studied as core medium for nonlinear light generation [31], tuneable ultrafast mode coupling [32, 33], or highly efficient guiding of mid-infrared laser light for medical applications [34–36]. Another largely overlooked halogenide liquid is tetrachloroethylene (C_2Cl_4, or TCE) which promises superior transmission from the visible towards the starting MIR [37] and a strong noninstantanous nonlinear response with a response time up to 4.6 ps [38]. Highly noninstantaneous media exhibit novel interesting phenoma such as strongly modified soliton dynamics [26] or temporarily induced anisotropies [39], and are therefore of great interest for both fundamental nonlinear optics and the development of new kind of custom-tailored light sources.

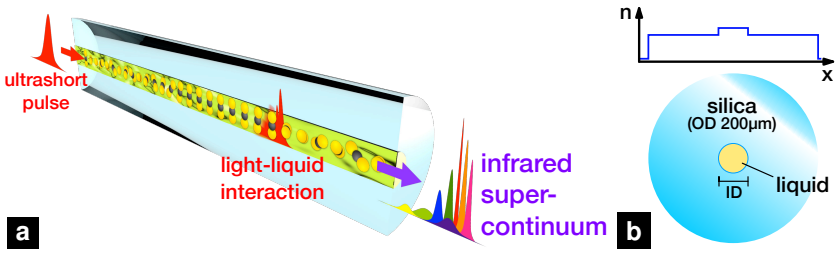

Fig. 1. (a) Illustration of the nonlinear interaction of an ultrashort optical pulses and the generation of new frequencies inside a liquid-core optical fiber. (b) Cross section of the liquid-core fiber type used in this work. The curve above the cross section illustrates the transversal refractive index distribution $n(x)$ of the step-index geometry. OD and ID stand for outer and inner diameter.

In this work we show that the solvents CCl_4 and C_2Cl_4 are highly interesting core materials for nonlinear infrared soft-matter photonics, which we demonstrate here by efficient supercontinuum generation at NIR wavelengths in straightforward-to-fabricate liquid-core silica fibers (see Fig. 1) pumped by an ultrafast thulium laser. We present corrected refractive index dispersion models for both liquids, enabling precise waveguide engineering and tailoring of phase-matched dispersive wave generation and soliton dynamics up to the starting MIR region. The dispersion models also allow for an accurate theoretical understanding of the measured supercontinua using generalized nonlinear pulse propagation simulations. Finally, we discuss the potential of carbon chloride waveguides for observing the hybrid dynamics of soliton fission, which represent a novel type of modified fission and propagation properties of solitary states resulting from highly noninstantaneous nonlinearities.

2. Material properties

The key prerequisite of effective supercontinuum generation (SCG) in optical fibers is the precise knowledge about (i) the effective index dispersion (i.e., group velocity dispersion (GVD)) (ii) the spectral domain of sufficient transmission, and (iii) the nonlinearity of the core material (i.e., the nonlinear refractive index (NRI) and the nonlinear response function (NRF)). In addition to low optical losses soliton-driven SCG requires anomalous GVD and an as high as possible nonlinearity. To evaluate the suitability of carbon chlorides as core material for efficient SCG, all three material properties are investigated in the following.

We measured the absorption of CS_2 (reference) and C_2Cl_4 similar to the measurement of CCl_4 by Kedenburg *et al.* [12] using a 1 m long tube closed on both sides by a sealed 1 mm thick silica window. The transmitted spectrum of a broadband fiber laser source (NKT SuperK) was measured with a fiber-coupled grating spectrometer (National Instruments, Spectro320) and corrected by

Optics EXPRESS

the wavelength-dependent reflection coefficients and a beam divergence correction function. The latter is gained from spectra measured with the detection fiber placed at different positions within the empty beam line (i.e. without tube). Spectral fluctuations of the supercontinuum source and flow-induced perturbations limit the sensing sensitivity to approximately 2 dB/m. The measurements (see Fig. 2(a-c)) reveal that both chlorides are highly transparent within the visible to the short wavelength infrared domain and are potentially even more transparent than the widely used material carbon disulfide (CS_2).

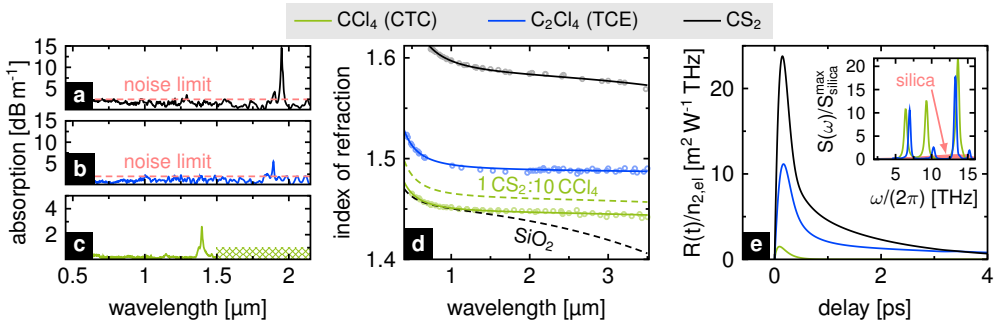

Fig. 2. (a-c) Measured absorption, (d) refractive index dispersion, and (e) nonlinear optical response of CS_2 (black), C_2Cl_4 (blue), and CCl_4 (green). The legend above the three plots applies to all diagrams. The absorption of CCl_4 in (c) is taken from Ref. [12], whereas no data are available within the crosshatched green area. The refractive index data in (d) are taken from multiple sources: CCl_4 from [12, 40–42], C_2Cl_4 from [42–45], CS_2 from [12, 40, 42, 46, 47]. The nonlinear responses in (e) do not contain the ultrafast Raman oscillations and are normalized to the respective electronic nonlinear refractive index $n_{2,el}$ at 1.92 µm wavelength. The inset shows the measured Raman spectrum $S(\omega)$ of CCl_4 and C_2Cl_4 normalized to the maximum gain peak of fused silica [48, 49]. The Raman data can be found in Data File 1 and Data File 2.

Precise models for the refractive index dispersion of the carbon chlorides are generally not well known. In fact, we found only one refractive index model for CCl_4 spanning from visible to near-infrared wavelength [12], which, however, omits the strong absorptions in the mid-IR. We therefore extended the known dispersion (Sellmeier) model $n^2 - 1 = \sum_{i=1}^{2} B_i\lambda^2/(\lambda^2 - C_i^2)$ by an additional term in the mid-IR for both liquids based on carefully fitting broadband refractive index data published earlier (see Fig. 2(d)). As we can see from the respective C_2 coefficients in Tab. 1 our models indeed include the first strong resonance in the mid-IR at 12.8 µm for CTC in accordance to Ref. [43] and at 11.0 µm for TCE in accordance to Refs. [42, 44].

For completeness, we also give the thermo-optical coefficients (TOC) $\partial n/\partial T$ at 20 °C, which are -5.50×10^{-4} K^{-1} for CCl_4 at 589 nm [50], and -6.23×10^{-4} K^{-1} for C_2Cl_4 at 600 nm [17]. For both liquids the spectral dispersion of the TOC is rather low, which may result from the overall flat refractive index dispersion of both media.

The NRI of molecular liquids is calculated by [28],

$$n_2 = n_{2,el} + n_{2,m} = n_{2,el} + \frac{\int I(t) \int I(t-\tau)R(\tau)\,\mathrm{d}\tau\mathrm{d}t}{\int I^2(t)\mathrm{d}t}\,, \tag{1}$$

where $n_{2,el}$ is the NRI originating from the electronic nonlinearity (i.e. instantaneous Kerr effect), $n_{2,m}$ is the NRI associated with the molecular nonlinearities, and $R(t)$ is the NRF of the molecule. Thus, Eq. (1) incorporates molecular motions induced by the light field of an excitation pulse with intensity distribution $I(t)$ and strongly depends on the initial pulse width. In the following,

Optics EXPRESS

the fraction $f_m = n_{2,\mathrm{m}}/n_2$ is referred as the molecular fraction or molecular contribution. Here, the general NRF presented by Reichert et al. is used [28]:

$$R(t) = \sum_k n_{2,k} r_k(t) + n_{2,\mathrm{L}} \underbrace{C_L \mathrm{e}^{-t/\tau_{\mathrm{d},L}} \Theta(t) \int_0^\infty \frac{\sin(\omega t)}{\omega} g(\omega)\, \mathrm{d}\omega}_{\text{normalization: } \int \ldots \mathrm{d}t = 1}, \tag{2}$$

with $r_k(t) = C_k(1 - \exp(-t/\tau_\mathrm{r}))\exp(-t/\tau_{\mathrm{d},k})\Theta(t)$ normalized to $\int r_k(t)\mathrm{d}t = 1$, the process-dependent decay time $\tau_{\mathrm{d},k}$, the rise time τ_r (assumed to be 100 fs as usually done in previous works), and the Heaviside function $\Theta(t)$. The last term accounts for the librational mechanism, which cannot be expressed by a simple overdamped function in the form of $r_k(t)$, but rather by an underdamped oscillation with a characteristic decay time $\tau_{\mathrm{d},L}$. As suggested by Reichert et al. for the case of CS_2 [28], we used an anti-symmetric Gaussian distribution $g(\omega) = \exp\left(-(\omega - \Omega)^2/(2\sigma^2)\right) - \exp\left(-(\omega + \Omega)^2/(2\sigma^2)\right)$ (central frequency Ω, spectral width σ) to fit the spectral resonance of this process.

For completeness we would like to mention that Raman oscillations can also straightforwardly be included into the NRF model by adding the normalized inverse Fourier transform of the Raman spectrum $n_{2,\mathrm{R}}\mathrm{Im}(\mathcal{F}^{-1}\{S(\omega)\})\Theta(t)$ to Eq. (2), where $S(\omega)$ is the Raman spectrum (see inset of Fig. 2(e)) normalized such that $\int \mathrm{Im}(\mathcal{F}^{-1}S(\omega))\Theta(t)\mathrm{d}t = 1$ and weighted by the NRI $n_{2,\mathrm{R}}$. The NRI $n_{2,\mathrm{R}}$ are given in the next paragraphs and were estimated based on Raman spectra of each liquid normalized to a silica reference (each measured in-house under identical conditions, i.e., using the same pump power, same sample lengths) and the known quantitative Raman model of silica [48, 49]. However, since Raman oscillations only become dominant at pulse widths below 100 fs (i.e., close to the cycle times of the oscillations) [27, 38] and since we use longer pulses (i.e., 270 fs and more), we safely neglect Raman contributions to the total NRI throughout this work without losing accuracy of the simulation results, as we confirmed by preliminary simulations.

Because of their different molecular shape, the dominating nonlinear processes and, thus, the nonlinear response of both liquids are fundamentally different. CTC features a quasi-isotropic molecular shape and its nonlinearity is dominated by instantaneous electronic excitations with small contributions from intermolecular dipole-dipole interactions ($n_{2,1} = 2 \times 10^{-20}\,\mathrm{m^2W^{-1}}$, $\tau_{\mathrm{d},1} = 150$ fs [51]) and intramolecular vibrational Raman oscillations ($n_{2,\mathrm{R}} = 1.6 \times 10^{-20}\,\mathrm{m^2W^{-1}}$). However, as mentioned before, the Raman contribution can be considered to be negligible here due to its relatively small amplitude and the ultrafast oscillation periods (e.g., 78 fs half-cycle

Table 1. Sellmeier coefficients (B_1, B_2, C_1, C_2), fit coefficient of determination (R^2), and nonlinear refractive indices ($n_{2,\mathrm{el}}$: electronic nonlinear index, $n_{2,\mathrm{m}}$: molecular nonlinear index (without Raman)) of CTC and TCE at 1.9 µm wavelength and FWHM pulse width of 300 fs.

	CCl_4 (CTC)	C_2Cl_4 (TCE)
B_1	1.09278717	1.21453712
B_2	0.10628401	0.03501419
C_1 [µm]	0.10937681	0.12064538
C_2 [µm]	12.79529912	11.09537922
R^2	0.9995	0.9982
$n_{2,\mathrm{el}}$ [10^{-20} $\mathrm{m^2W^{-1}}$]	4.6551	5.5302
$n_{2,\mathrm{m}}$ [10^{-20} $\mathrm{m^2W^{-1}}$]	0.6634	11.2267

Optics EXPRESS

time of the slowest response at 213 cm^{-1}) being much faster than the pulse width used in this work. Furthermore, the NRF (see Fig. 2(e)) does not feature reorientation or libration components (i.e., $n_{2,2} = 0$ and $n_{2,L} = 0$ [51]). The final temporal nonlinear response of CTC possesses a rather fast dynamic, which can be seen as quasi-instantaneous due to its small molecular contribution (e.g., $f_m = 0.18$ for a pulse width of 300 fs).

In contrast, TCE is a prolate molecule, which causes an intensity dependent anisotropy based on molecular reorientation in a linearly polarized light field. No quantitatively accurate model for TCE is available in the literature, whereas it is not straightforward to deduce one from the few data published. However, we were able to estimate (i) the relative amplitudes of the noninstantaneous components via successive fitting of the individual terms of Eq. (2) to z-scan data published by Thantu et al. [38], and (ii) the molecular fraction f_m for 80 fs pulses with own in-house NRI and z-scan measurements. Our fitting procedure results in a model with two overdamped responses (dipole-dipole interactions: $n_{2,1} = 3.1 \times 10^{-20}\,m^2W^{-1}$, $\tau_{d,1} = 2.98$ fs; diffusive reorientation: $n_{2,2} = 50.1 \times 10^{-20}\,m^2W^{-1}$, $\tau_{d,2} = 4.5$ ps), a residual underdamped term (libration: $n_{2,L} = 20.8 \times 10^{-20}\,m^2W^{-1}$, $\tau_{d,L} = 780$ fs, $\Omega = 4.0$ THz, $\sigma = 6.3$ THz), and a small Raman contribution ($n_{2,R} = 0.9 \times 10^{-20}\,m^2W^{-1}$), which we neglected in further considerations. The resulting response in Fig. 2(e) shows that TCE has a highly noninstantaneous temporal response (e.g., with a molecular contribution of $f_m = 0.67$ in case of a 300 fs excitation pulse), as it becomes obvious by comparing TCE, the quasi-instantaneous CTC and the highly noninstantaneous CS_2.

3. Fiber design

The dispersions and nonlinear parameters of the fundamental fiber modes have been calculated semi-analytically using the dispersion equation of a step-index fiber [52, 53]. In case of TCE, the refractive index at our operation wavelength 1.92 µm is large enough ($n_{C_2Cl_4} = 1.489$) to serve as a robust waveguide (e.g., numerical aperture $NA = 0.38$). In case of CTC, however, its refractive index is very close to that of the silica cladding ($n_{CCl_4} = 1.447 \approx n_{SiO_2} = 1.439$) and guiding in the neat solvent might become critical with regard to bends, waveguide inhomogeneities, and temperature fluctuations ($NA = 0.15$). To improve the index contrast, we added 10 vol% of CS_2 to CCl_4 to increase the refractive index to $n_{CS_2/CCl_4} = 0.1n_{CS_2} + 0.9n_{CCl_4} = 1.461$ [54] allowing more robust wave guiding ($NA = 0.25$).

Using our material dispersion models (from Tab. 1), we calculated the nonlinear coefficient as function of wavelength and core diameter $\gamma(\lambda, R)$ for both liquids (see Fig. 3) including the dependence of the zero-dispersion wavelength (ZDW; i.e., the wavelengths at which the GVD switches its sign), the single-mode criterion (i.e. guidance parameter of $V = 2.405$), and the critical guidance limit ($V_{crit} = 1.2$) analogously to [53]. The nonlinear parameter, thereby, contains the total NRI incorporating the individual nonlinear response functions $R(\tau)$ via Eq. (1) assuming a FWHM pulse width of 300 fs similar to our experiment.

The nonlinear maps in Fig. 3 give intuitive impressions of the design possibilities of step-index LCFs. Similar to glass-based fibers the single-mode criterion gives a good approximation for the design parameters exhibiting maximum nonlinearity [53]. We also see that the evolution of the ZDW is significantly different for both liquids due to the different refractive indices. CTC shows an intuitive monotonic shift of the modal ZDW from the ZDW of bulk silica (i.e. the cladding) towards the ZDW of the bulk liquid with increasing core diameter. TCE, instead, features another ZDW minimum at comparably large core diameters of 4 to 5 µm and, thus, large V parameters (i.e., geometries for efficient coupling and guidance) being comparable to the ZDW minimum observed for CS_2 [26]. This local minimum is suitable for SCG using a thulium laser with an operation wavelength of about 2 µm. The purple marks in Fig. 3 show the working points used in our experiments, which allow to operate in the anomalous dispersion region and close to the single-mode criterion and, in case of the 4.6 µm core diameter fibers, close to the maximum

Optics EXPRESS

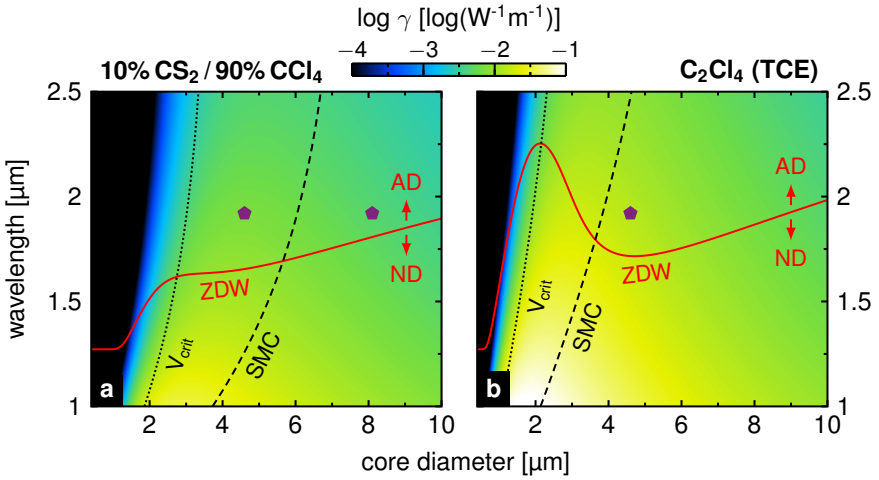

Fig. 3. Design maps of silica-cladding LCFs filled with (a) a 10 vol% CS_2 / 90 vol% CCl_4 mixture or (b) TCE. The contour plots show the decadic logarithm of the nonlinear coefficient as functions of wavelength and core diameter. The purple marks label the experimental configurations used in this work. Red line: zero-dispersion wavelength (ZDW); black dashed line: single-mode criterion (SMC); dotted black line: critical waveguide parameter (V_{crit} = 1.2). AD and ND refers to anomalous and normal dispersion, respectively.

nonlinear parameter for 1.92 µm pump wavelength.

4. Setup and simulations

The SCG-experiments were based on a setup that combines an ultrafast thulium laser source with a optofluidic system (see scheme in Fig. 4). The laser source comprises a commercial thulium-based fiber oscillator delivering pulses with 500 fs duration centered at 1.92 µm at a repetition rate of 25 MHz. These pulses are stretched in 25 cm anomalous dispersive single-mode fiber (Corning SMF-28) and 4 m normal dispersive ultra-high NA fiber (Thorlabs UHNA4), and polarization controlled by a combination of half- and quarter-wave-plate. Finally, this (seed) signal with around 3 mW average power was coupled to a thulium-doped photonic crystal fiber with 35 µm mode-field diameter, and desirably amplified to 0.5 - 1.0 W. The initial negative chirp is compensated in the anomalous dispersive amplifier fiber and, furthermore, nonlinearly compressed down to approximately 300 fs full-width half-maximum (FWHM) pulse duration. The output pulse shape and spectrum of the laser system were controlled online with two reflexes coupled into an autocorrelator and a spectrometer at any time of the experiments, ensuring stable pulse conditions. The inset of Fig. 4 compares the measured and reconstructed autocorrelations corresponding to a 270 fs $sech^2$ pulse with a residual β_3-phase of 7×10^6 fs^3.

The LCFs are fabricated by mounting a silica capillary with a well-selected inner diameter in two optofluidic mounts (OFM, i.e. small tanks made of aluminum with sealed optical windows (1 mm thick sapphire window) and inlet, outlet and fiber ports). In each OFM the capillary body is sealed by a sleeve-ferrule connection inside the fiber port. The OFMs were then flushed successively with the solvent under a fume hood, and the inlet and outlet ports of each filled OFM (approximately 1 µl per mount) were sealed by port blocks made of fluoropolymer. The OFMs are placed on or in front of a fiber coupling stage (i.e. a three-axis translation stage) and the laser was coupled free-space with aspheric lenses (Thorlabs A375 at input, C230 at output). Efficient coupling to the fundamental mode was ensured using an extended InGaAs camera to monitor

Optics EXPRESS

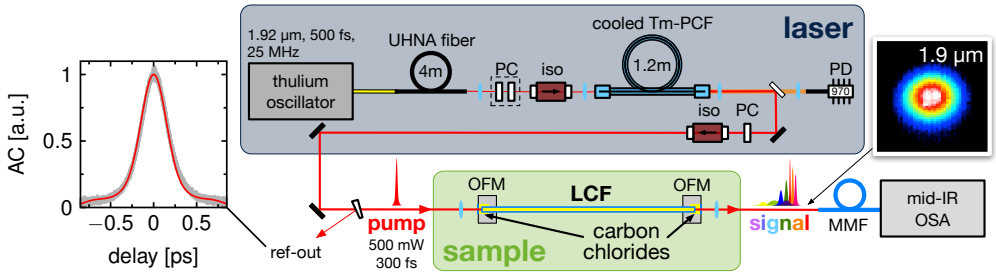

Fig. 4. Scheme of the laser setup and the optofluidic supercontinuum generation setup. The reference output (ref-out) are two reflexes from a wedge coupled into spectrometer and auto-correlator (AC). One measured AC traces is exemplarily shown in the inset (gray marks) and compared to the calculated AC of the pulse reconstructed from the measured spectrum (red line). PC: polarization control, PD: pump (laser) diode, OFM: optofluidic mount, LCF: liquid-core fiber, MMF: multimode fiber. The inset on the right-handed side shows a near-field image of the output fundamental mode at 1.9 µm wavelength.

the output mode. After coupling optimization, the fiber output was collimated (for the pump wavelength) and detected with a 100 µm InF_3 multimode fiber directly placed in the collimated beam and linked to suitable spectral analyzers (Yokogawa NIR and MIR OSA). In a typical measurement we recorded the output spectra for various pulse energies while we accurately controlled input and output power during all measurements. The pulse energy in each experiment was increased until the transmission efficiency dropped, defining the damage threshold of the respective fiber.

Results are confirmed and interpreted by the use of nonlinear pulse propagation simulations based on the generalized nonlinear Schrödinger equation (GNLSE)

$$\partial_z \tilde{A}(z;\omega) - \mathrm{i}\left[\beta(\omega) - \beta_0 - \omega\beta_1\right]\tilde{A} = \mathrm{i}\bar{\gamma}(\omega)\,\mathcal{F}\left\{A(z,t)\int_{-\infty}^{\infty} h(t')|A(z,t-t')|^2\mathrm{d}t'\right\}, \qquad (3)$$

where $\tilde{A}(z;\omega) = \mathcal{F}\{A(z;t)\}$ is the spectral field amplitude, i.e., the Fourier transform of $A(z;t)$, $\beta(\omega)$ is the propagation constant including the dispersion over the entire bandwidth set into the moving frame with $\beta_0 = \beta|_{\omega_0}$ and $\beta_1 = \partial_\omega\,\beta|_{\omega_0}$, and $\bar{\gamma}(\omega)$ is the broadband nonlinear parameter including the mode overlap correction by Laegsgaard [55]. Absorption is neglected due to the high transmission of both liquids. The response function is $h(t) = (1 - f_\mathrm{m})\delta(t) + f_\mathrm{m}\bar{R}(t)$ with the molecular fraction f_m and the rescaled NRF $\bar{R}(t)$ normalized such that $\int \bar{R}(t)\mathrm{d}t = 1$. The simulations are performed with a chirp-free 270 fs pulse with an sech^2 intensity shape, whose autocorrelation width is close to the measured autocorrelation in the experiment (see inset of Fig. 4).

5. Soliton fission in CTC

We started our experiments with a LCF with a core diameter of 4.6 µm (length 25 cm, guidance parameter $V(1.92\,\mu\mathrm{m}) = 1.88$) filled with the composition 10 vol% CS_2/90 vol% CCl_4. A coupling efficiency of 35 % was achieved assuming 15 % measured reflection and clipping losses at the input lens, 6 % reflection losses at the output lens, 7.3 % reflection loss at each of the two sapphire windows, and lossless propagation. The spectral power evolution in Fig. 5(a) reveals a first breathing cycle of a higher-order soliton until 1 nJ, i.e., a slight spectral broadening until energies of 0.8 nJ followed by spectral narrowing, until a red-shift dominates for higher pulse energies.

Optics EXPRESS

The maximum soliton number of the system is about 6.6. The observed behavior is characteristic for higher-order soliton splitting, i.e., soliton fission in case of propagation in a highly dispersive domain far away from the ZDW [52, 56]. The power dependence of the spectral evolution is well reproduced by the nonlinear simulations (see Fig. 5(b)), which also indicate the emergence of a distant dispersive wave (DW; also known as non-resonant, or Cherenkov radiation) at 1.15 µm which lies outside of our measured spectral domain (red domain in Fig. 5(a)). The appearance of the DW after the first spectral breathing cycle is a clear indicator for a higher-order soliton propagation perturbed by third-order dispersion, which initiates the decomposition of the soliton breather.

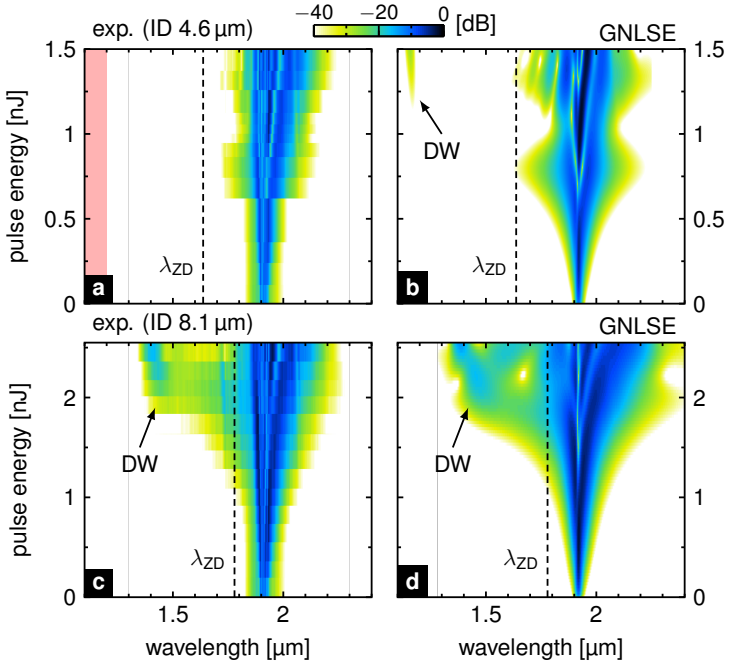

Fig. 5. Measured (left column) and simulated (right column) power spectral distribution of supercontinua generated in two CCl_4-filled LCFs with different core diameter and slightly different length ((a, c) 4.6 µm, 25 cm, (b, d) 8.1 µm, 20 cm). The color scale is identical for all panels and refers to the normalized decadic logarithm of the intensity in dB.

Using our design map from Fig. 3(a), we test the SCG capabilities of the CTC-LCF at low pump energies by shifting the ZDW closer to the pump wavelength by increasing the core diameter to 8.1 µm (thus $V(1.92\,\mu m) = 3.31$). The used LCF sample had a length of 20 cm, and coupling efficiencies up to 55 % have been reached. The measured power spectral evolution in Fig. 5(c) shows a distinct DW at 1.4 µm at a pump energy of 2 nJ and a spectral broadening up to 850 nm bandwidth at maximum pulse energy, which is again well described by the GNLSE simulations in Fig. 5(d). The maximum soliton number of this system is 12 and thus higher than in the previous system with the smaller core despite the lower nonlinear parameter (see Fig. 3(a)).

The fact that the maximum launchable pulse energy is higher for the second large-core configuration compared to the first situation falsely suggests that the type of damage causing the transmission drop is related to the peak power rather than to the injected pulse energy. However, the damage threshold of both fibers is comparable when we consider the damage to happen at the fiber input facet, where the highest field intensity is located. By calculating the pulse energies

Optics EXPRESS

before coupling taking into account the respective coupling efficiencies and highest pulse energies (see Fig. 5) we find values around 4.5 nJ for both fibers, which corresponds to a peak power limit of approximately 15 kW at 1.92 µm. Peak powers nearly twice that high are achieved during the nonlinear self-compression just before soliton fission which we measured without stability problems. Therefore, we assume that the observed drop of the transmission is not linked to the injected intensity but rather to pulse energy or accumulated thermal load.

6. Supercontinuum generation in TCE

In case of the TCE-LCF (core diameter: 4.6 µm, $V(1.92\,\mu m) = 2.86$, fiber length: 21 cm) the spectral evolution shown in Fig. 6(a) changes drastically with input power. A clean soliton fission process with a low onset energy of just 0.5 nJ is observed indicated by the clean shear-off of a DW at 1.35 µm. Increasing pulse energy yields the following observations: (i) the spectral bandwidth increases towards both sides of the pump, (ii) more spectral features arise in the "dark valley" between DW and pump suggesting the successive fission of more solitary waves, and (iii) a fine structuring appears in the spectral signatures of both DW and the solitary wave on the long-wavelength side (see highlighted domains in Fig. 6(a)) indicating temporal interference between different spectral components. The entire spectral power evolution, featuring its slow transition to an octave spanning supercontinuum and its fine spectral fringes, is well reproduced by the nonlinear simulations based on the GNLSE in Fig. 6(b), which is remarkable considering the coarse estimation of the NRI and the NRF of TCE discussed above.

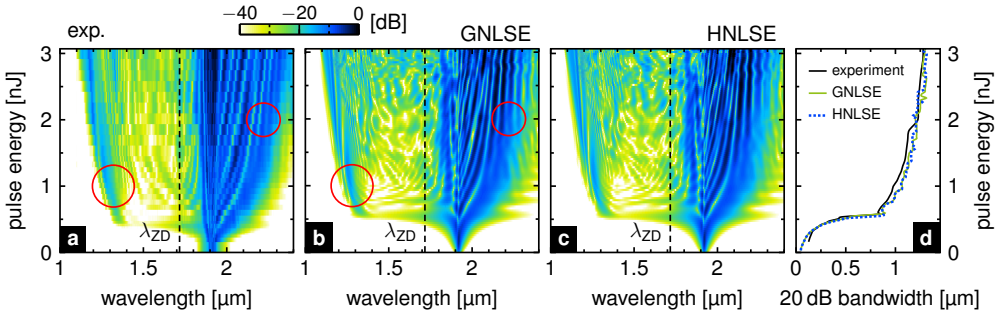

Fig. 6. (a) Measured spectral distribution of supercontinuum generation after 21 cm C_2Cl_4-LCF for increasing pulse energy. (b) Corresponding simulated spectral power evolution obtained by solving (b) the GNLSE and (c) the HNLSE assuming a 270 fs $sech^2$ input pulse (details can be found in main text). (d) Comparison of the 20 dB bandwidth of the generated supercontinua between measurement and the two numerical solvers.

7. Impact of noninstantaneous phase

It was shown in previous work that optical solitary solutions in LCFs might be drastically modified by the highly noninstantaneous nonlinear response of the liquid [29], which, in particular, leads to novel properties of the fission process such as a substantially reduced susceptibility to phase noise, reduced spectral bandwidths, and an increased onset energy [26]. Although the latter two are not beneficial from the application point of view, the strong robustness with regard to system noise promises a drastically improved pulse-to-pulse spectral stability for input pulses with duration of hundreds of femtoseconds. Such stability is not accessible with full-glass systems, opening a new realm for ultra-stable reconfigurable supercontinuum sources for shot-to-shot spectroscopy and microscopy.

Optics EXPRESS

We tested our hypothesis with CS_2, which possesses a very strong and highly noninstantaneous NRF with a large molecular contribution to the total nonlinearity of the medium as visible in Fig. 2(e). However, CS_2 has a number of disadvantages particular from the application perspective, which are a comparably high toxicity and strong absorption towards 3.5 µm, limiting the propagation length to further study the modified soliton dynamics in the near- to mid-IR domain. TCE instead is less toxic and presumably much more transparent since its vibrational transitions are at longer mid-IR wavelengths, making it an ideal core material for wide-spread use in nonlinear photonics. Moreover, TCE possesses a similarly strong noninstantaneous response as CS_2 (see Fig. 2(e)) which is not the case for quasi-instantaneous CTC.

To understand the impact of the noninstantaneous phase, we used the hybrid nonlinear Schrödinger equation (HNLSE) derived in our previous work [26]

$$\partial_z \tilde{A}(z;\omega) - \mathrm{i}\bar{\beta}(\omega)\tilde{A} = \mathrm{i}\bar{\gamma}(\omega)\,\mathcal{F}\left\{\left[(1-f_m)|A(t)|^2 + f_m V_0(t)\right]A(z;t)\right\} \tag{4}$$

with $\bar{\beta}(\omega) = \beta(\omega) - \beta_0 - \omega\beta_1$ as effective propagation constant in the moving frame of the initial pulse at frequency ω_0. Equation (4) is a considerably simpler version of the GNLSE in Eq. (3), since the run-time consuming convolution integral is replaced by an initial linear (convolution) potential $V_0(t) = \bar{R}(t) * |A(0;t)|^2$, which is calculated only once at the start of the numerical solver (i.e. at $z = 0$). We applied the HNLSE to our current experiment and found a perfect agreement to the simulations using the GNLSE (compare Fig. 6(b) and (c)). In particular the comparison of the 20 dB bandwidths between experiment and both simulations in Fig. 6(d) shows an almost perfect match. However, a closer investigation of the results revealed that the noninstantaneous phase has in fact a negligible influence on the broadening process, as simulations using Eq. (4) with $V_0 = 0$ result in exactly the same broadening behavior (not shown here). Thus, mainly instantaneous nonlinear processes drive the spectral broadening observed in our recent TCE experiments, which is in contrast to our previous findings gained with 450 fs pulses in CS_2-LCFs.

This discrepancy originates from the dependence of the molecular contribution to the total nonlinearity on pulse width, which impacts the strength of the noninstantaneous (nonlinear) phase (NIP) relative to the instantaneous Kerr phase (IKP). The IKP can be expressed in first approximation by $\varphi_{\mathrm{IK}} = (1-f_m)\gamma_0 P_0$ with $\gamma_0 = \gamma(\omega_0)$ and peak power P_0, the NIP by $\varphi_{\mathrm{NI}} = f_{\mathrm{m}}\gamma_0 V_{0,\max}$ with $V_{0,\max} = \max(V_0(t))$. Comparing the NIP with the IKP for increasing pulse width in Fig. 7(b) shows that in contrast to CTC, the two liquids CS_2 and TCE feature a point where the NIP exceeds the IKP, i.e., where the soliton dynamics are strongly modified by the noninstantaneous nonlinear response of the molecules. This transition point, however, appears at a much longer pulse widths in case of TCE ($T_{\mathrm{FWHM}} = 600$ fs) than in case of CS_2 ($T_{\mathrm{FWHM}} = 210$ fs). This effect is related to the weaker amplitude of the noninstantaneous response of TCE (see Fig. 2(e)) and a three times longer decay time of the molecular reorientation [38].

Despite the longer response times, the potential of TCE as efficient medium for promoting modified soliton dynamics is still immanent and can be made visible when being compared to an entirely instantaneous system. For example, we investigate the spectral evolution of a 1.9 ps pulse (here a strongly chirped 270 fs pulse), which results in a dominant NIP clearly above the transition point from the IKP-dominant regime and being comparable to the NIP in our previously published demonstration using CS_2 [26] (see set points in Fig. 7(b). We numerically investigate lossless pulse propagation along 2 m of fiber with equivalent GVD but different nonlinear response accordingly to either (i) a glass-type fiber with smaller and entirely instantaneous nonlinearity $(1-f_{\mathrm{m}})\gamma_0$ and (ii) a C_2Cl_4-LCF with realistic response. Mathematically, we compare two numerical solutions of the GNLSE in Eq. (3) for the same type of fiber with either a vanishing ($\bar{R}(t) = 0$, case i) or a non-zero (case ii) noninstantaneous response. Since nonlinear light generation relying on picosecond pulses is highly susceptible to phase noise we add white quantum noise (i.e. one photon per frequency channel with random phase) to the initial pulse spectrum, which is a widely accepted model to include noise effects [56].

Optics EXPRESS

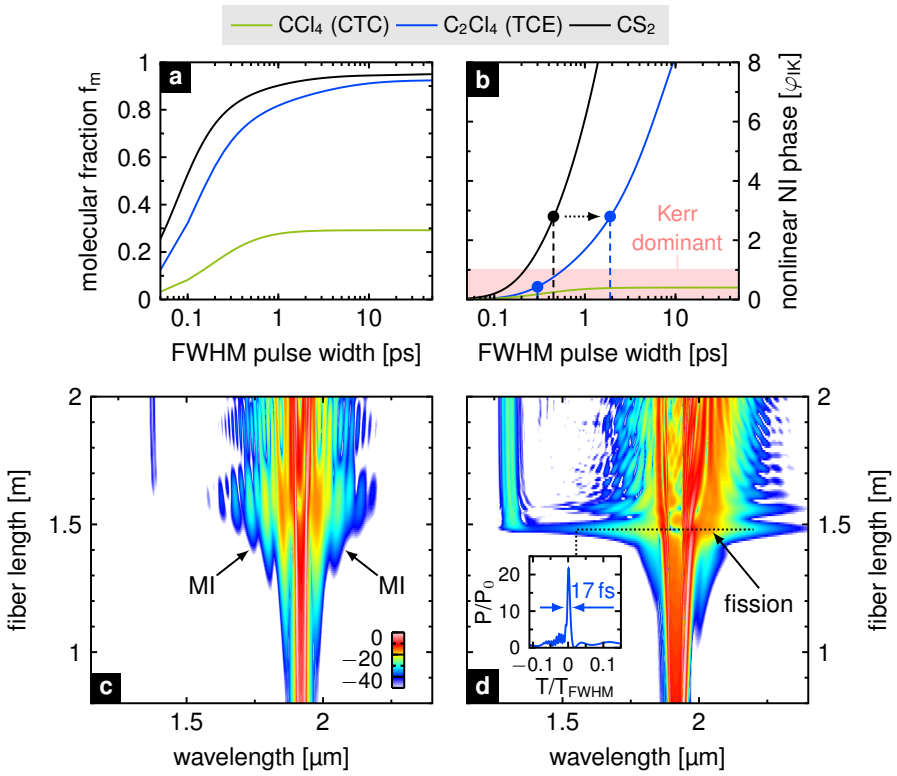

Fig. 7. (a) Noninstantaneous contribution to the total nonlinearity and (b) maximum of the noninstantaneous phase from Eq. (4) normalized to the maximum of the Kerr phase $\varphi_{\mathrm{IK}} = (1 - f_m)\gamma_0 P_0$ as function of temporal input pulse width for the three solvents. The marks highlight the working points of previous work in CS_2 [26] and this work. (c-d) Spatial-spectral evolution of a strongly chirped 1.9 ps pulse with 500 W peak power numerically calculated on basis of the GNLSE (c) without and (d) with noninstantaneous phase (the color scale refers to the normalized decadic spectral intensity in dB). The spectral modulations in (c) clearly indicate modulations instabilities (MI) as the dominant broadening process, whereas the C_2Cl_4-LCF system in (d) shows clean soliton fission and dispersive wave generation. The inset in (d) shows the pulse power (normalized to the input peak power) over time (normalized to the FWHM width of the input pulse) at the maximum compression point.

The instantaneous glass-type system (case i) develops characteristic spectral modulations (labeled "MI" in Fig. 7(c)) originating from modulation instabilities (i.e. the random rise of multiple, similarly strong temporal confinements), which is a commonly known noise-triggered effect for picosecond pulses propagating in the anomalous dispersion domain [9,56]. The spectral characteristics of the symmetric side lobes and the signature of the DWs are different from run to run (e.g., Fig. 7(c) shows both signatures in the spectral evolution of one individual simulation) due to initial phase fluctuations causing the formation of solitary states in random temporal and spectral windows of the pulse. The noninstantaneous TCE system (case ii), in contrast, shows a clean fission process of an initial soliton indicated by the modulation-free symmetrically broadened pedestal and the emission of an intense DW after 1.5 m propagation in Fig. 7(d). Remarkably, the pulse is compressed by two orders of magnitude down to 17 fs (FWHM width) at the fission point resulting in a peak power enhancement of factor 22 (inset of Fig. 7(d)). The

Optics EXPRESS

peak power enhancement is multiple times larger than in case of the solitary features resulting from modulation instabilities, with the consequence that energy is effectively transferred to the DW and its phase-matching point is shifted towards the blue [56].

Simulating an ensemble of 20 spectra each with different initial phase noise shows that, despite the presence of noise, the spectra of the LCF system are highly correlated (i.e., the shot-to-shot spectral variations are small expressed in a high spectrally averaged coherence $\langle|g_{12}^{(1)}|\rangle = 0.93$), which is in great contrast to the broadening process in the instantaneous glass-type systems (with smaller coherence $\langle|g_{12}^{(1)}|\rangle = 0.66$). The origin of this improved coherence property is associated with the strong influence of the high noninstantaneous nonlinearity. The pulse undergoes a phase rectification process during the propagation through the non-instantaneous medium. This effect might be comparable to an optical memory effect, that is, the characteristics of a pulse section are encoded in the induced nonlinear polarization of the slow molecular motions and couples back to all later parts of the pulse. This leads to an averaging of the phase noise along the pulse during propagation and, thus, to a clean soliton fission, which is in general a highly phase sensitive process.

The reader should note that the model of the nonlinear response of TCE used in this work is a course estimation and is not as reliable as the nonlinear model of CS_2 given in [28]. A future correction of the model might impact the parameter domains shown in Fig. 7, whereas, however, the basic findings will remain. We simulated the impact of response model variations on our results presented in Fig. 6(b,c) and Fig. 7(d), e.g., by reducing or amplifying the amplitude of the nonlinear response by a factor one half or two, respectively, showing no significant change of the results. Thus, we are convinced that our theoretical findings in combination with the measurements are based on solid grounds.

8. Conclusion

In conclusion, we have shown soliton fission and broadband supercontinuum generation at short-wave infrared wavelengths in halide based liquid-core fibers experimentally and numerically. We reviewed and partially derived models for the linear and nonlinear refractive index of both liquids used (i.e., carbon tetrachloride (CCl_4) and tetrachloroethylene (C_2Cl_4)), which enabled accurate fiber design of liquid-core silica-cladding fibers. We observed soliton fission and the emission of dispersive waves for both liquid-core fibers using 270 fs pulses at 1.92 µm wavelength. In particular the C_2Cl_4-core fiber showed octave-spanning bandwidths (maximum: 1.1 µm to 2.4 µm) with the broadening starting at pulse energies as low as 0.5 nJ. The good match between expectations based on design calculations, experimental data and simulations based on the nonlinear Schrödinger equation confirm the good quality of our models for dispersion and nonlinearity. In fact the models allow for accurate dispersion design and tailoring of soliton dynamics in halide-core fibers on a level which is comparable to that of silica fibers.

Finally, we demonstrated the potential of C_2Cl_4 for observing a new type of soliton dynamics – so-called hybrid soliton dynamics – resulting from the highly noninstantaneous nonlinear response of certain liquids, which was recently demonstrated for CS_2-core fibers [26]. Due to potentially lower absorption towards the mid-IR (below the noise limitations of our spectrometric setup) C_2Cl_4-core fibers might allow for much longer propagation lengths than CS_2-core fibers thus promising access to the fundamental soliton domain in future work. However, the noninstantaneous nonlinearity of C_2Cl_4 is weaker and much more delayed compared to CS_2. Thus, its impact starts to become dominant at longer pulse widths (i.e., longer than 600 fs) which we estimated by comparing the nonlinear phase terms of a simplified form of the nonlinear Schrödinger equation. We exemplarily showed that C_2Cl_4-core fibers can significantly reduce noise-dictated nonlinear effects of picosecond pulse propagation such as modulation instabilities and might enable reliable self-compression of picosecond pulses down to the few-cycle regime. Even though the model of the nonlinear response of C_2Cl_4 has to be confirmed by future pump-probe experiments, it

Optics EXPRESS

explains the observations of the experiments presented with remarkable agreement to simulations. Hence, we are convinced that our nonlinear model is reasonable and will enable progress in device design for mid-infrared photonics. Future studies need to clarify whether noninstantaneous effects are able to outperform in noise-sensitive light generation, ascribing a key role to noninstantaneous liquids such as C_2Cl_4 for reducing the impact of phase and quantum noise in optical systems.

Funding

German Research Foundation (DFG) (SCHM2655/3-1, International Research Training Group (IRTG) via grant GRK 2101/1); Thuringian State (2015FGI0011, 2015-0021) partly supported by the European Social Funds (ESF); and the European Regional Development Fund (ERDF); University of Central Florida (Project "Fundamental Fiber Laser Science for High Powers" Award Number 321095).

Acknowledgments

We thank Dr. Christian Karras, Dr. Wolfgang Paa, and Dr. Herbert Stafast for providing z-scan data of TCE, CS_2 and silica. We thank Dr. Andreea Radu for providing Raman data of CTC, TCE, and silica. Fabian Stutzki acknowledges support by the Carl-Zeiss-Stiftung. Martin Gebhardt acknowledges support by the Helmholtz-Institute Jena.